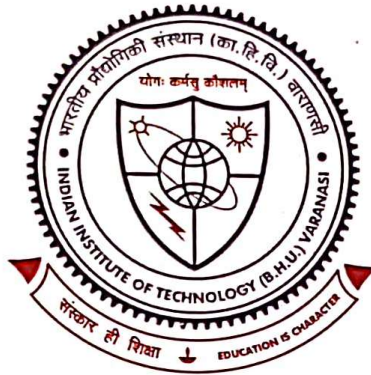


Low Frequency Oscillations Damping in Power Networks Through PSS and Robust Wide-Area Damping Controller



Thesis submitted in partial fulfillment
for the award of degree

Doctor of Philosophy

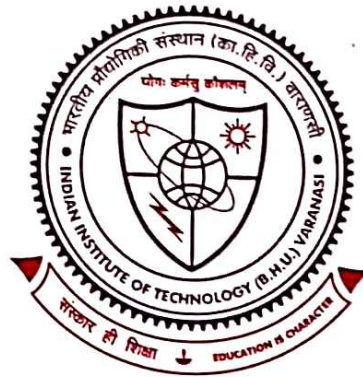
by

Rohit Kumar

DEPARTMENT OF ELECTRICAL ENGINEERING
Indian Institute of Technology
(Banaras Hindu University)
Varanasi

Roll No: 18081502

Low Frequency Oscillations Damping in Power Networks Through PSS and Robust Wide-Area Damping Controller



Thesis submitted in partial fulfillment
for the award of degree

Doctor of Philosophy

by

Rohit Kumar

DEPARTMENT OF ELECTRICAL ENGINEERING

Indian Institute of Technology

(Banaras Hindu University)

Varanasi

Roll No: 18081502

CERTIFICATE

It is certified that the work contained in the thesis titled **Low Frequency Oscillations Damping in Power Networks Through PSS and Robust Wide-Area Damping Controller** by author has been carried out under my/our supervision and that this work has not been submitted elsewhere for a degree.

It is further certified that the student has fulfilled all the requirements of Comprehensive Examination, Candidacy, and SOTA for the award of Ph.D. Degree.



Supervisor

Prof. Mitresh Kumar Verma

Deptt. of Electrical Engg.

IIT(BHU), Varanasi

Varanasi, India - 221005

विद्युतीय अभियान्तिकी विभाग / Department of Electrical Engineering
भारतीय प्रौद्योगिकी संस्थान / Indian Institute of Technology
(काशी हिन्दू विश्वविद्यालय) / (Banarusi Hindu University)
Varanasi, U.P. (INDIA)



Co-Supervisor

Prof. Soumya R Mohanty

Deptt. of Electrical Engg.

IIT(BHU), Varanasi

Varanasi, India - 221005

विद्युतीय अभियान्तिकी विभाग / Department of Electrical Engineering
भारतीय प्रौद्योगिकी संस्थान / Indian Institute of Technology
(काशी हिन्दू विश्वविद्यालय) / (Banarusi Hindu University)
Varanasi, U.P. (INDIA)

DECLARATION

I, **Rohit Kumar**, certify that the work embodied in this thesis is my own bonafide work and carried out by me under the supervision of **Prof. Mitresh Kumar Verma** and **Prof. Soumya R Mohanty** from January-2019 to July-2024, at the Departement of Electrical Engineering, Indian Institute of Technology (BHU), Varanasi. The matter embodied in this thesis has not been submitted for the award of any other degree/diploma. I declare that I have faithfully acknowledged and given credits to the research workers wherever their works have been cited in my work in this thesis. I further declare that I have not willfully copied any other's work, paragraphs, text, data, results, etc., reported in journals, books, magazines, reports dissertations, theses, etc., or available at websites and have not included them in this thesis and have not cited as my own work.

Date: 6.1.2025

Rohit Kumar

Place: Varanasi

(Rohit Kumar)

CERTIFICATE BY THE SUPERVISOR

It is certified that the above statement made by the student is correct to the best of my/our knowledge.


Supervisor

Prof. Mitresh Kumar Verma

IIT(BHU), Varanasi

PROFESSOR
विद्युतीय अभियांत्रिकी विभाग / Department of Electrical Engineering
भारतीय प्रौद्योगिकी संस्थान / Indian Institute of Technology
(काशी हिन्दू विश्वविद्यालय) / (Banaras Hindu University)
Varanasi, U.P. (INDIA)

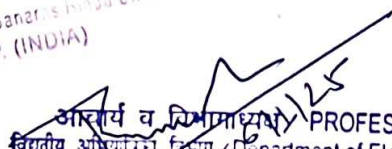


Co-Supervisor

Prof. Soumya R Mohanty

IIT(BHU), Varanasi

PROFESSOR
विद्युतीय अभियांत्रिकी विभाग / Department of Electrical Engineering
भारतीय प्रौद्योगिकी संस्थान / Indian Institute of Technology
(काशी हिन्दू विश्वविद्यालय) / (Banaras Hindu University)
Varanasi, U.P. (INDIA)


Signature of Head of Department / Coordinator of School
PROFESSOR & HEAD
विद्युतीय अभियांत्रिकी विभाग / Department of Electrical Engineering
भारतीय प्रौद्योगिकी संस्थान / Indian Institute of Technology
(काशी हिन्दू विश्वविद्यालय) / (Banaras Hindu University)
Varanasi, U.P. (INDIA)

COPYRIGHT TRANSFER CERTIFICATE

Title of the Thesis: **Low Frequency Oscillations Damping in Power Networks Through PSS and Robust Wide-Area Damping Controller**

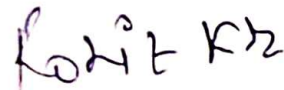
Name of Student: **author**

Copyright Transfer

The undersigned hereby assigns to the Indian Institute of Technology (Banaras Hindu University), Varanasi all rights under copyright that may exist in and for the above thesis submitted for the award of the Doctor of Philosophy.

Date: **6.1.2025**

Place: **Varanasi**



(Rohit Kumar)

Note: However, the author may reproduce or authorize others to reproduce material extracted verbatim from the thesis or derivative of the thesis for author's personal use provided that the source and the Institute's copyright notice are indicated.

Acknowledgment

First and foremost, I would like to express my gratitude to **Lord Vishwanath Ji** for the countless blessings, knowledge, and opportunities bestowed upon me, enabling me to complete this thesis. While my name appears on the cover of this dissertation, the success of this work is due to the support and guidance of many others. I owe my heartfelt thanks to everyone who made this thesis possible and contributed to a research experience I will cherish forever.

I extend my deepest gratitude to my supervisor, **Prof. Mitresh Kumar Verma** and co-supervisor, **Prof. Soumya R. Mohanty**, from the Department of Electrical Engineering at IIT (BHU) Varanasi, for their unwavering support, guidance, and patience throughout my research. It has been a privilege to work under their mentorship.

I also thank the Head of the Department of Electrical Engineering, IIT (BHU), Varanasi, for providing all the facilities necessary for my research work. My sincere thanks go to **Prof. S.P. Singh** and **Prof. R.K. Pandey** for their unconditional support during my research journey. I also appreciate the other faculty members of my research progress evaluation committee, **Dr. J.C. Pandey** and **Prof. Subir Das**, for their invaluable support and constant encouragement throughout the research period. I am grateful to **Dr. Avirup Maulik**, **Prof. Sandip Ghosh**, and **Dr. Subho Paul** for their support and for helping me maintain high standards in my work. I extend my heartfelt thanks to all the faculty members of the Electrical Engineering Department. I am grateful to my friend, **Dr. Shailendra Singh**, **Mr. Abhishek Singh** and **Mr. Ambuj Pandey**, who provided me with technical, moral, and emotional support during my research program.

I am also thankful to our laboratory staff, **Mr. Sanjay Bharti**, **Mr. Dharmendra Singh**, and **Mr. Vinish Singh**, for their assistance during this research. My gratitude goes to all the office staff and authorities of the Department of Electrical Engineering for their help during my stay to complete the thesis work.

A special thanks to my colleagues, including Dr. Manohar Singh, Dr. Anil Kumar Thakur, Dr. Devesh Shukla, Dr. Akhilesh Barnwal, Dr. Lokesh Yadav, Dr. Vivek Kumar, Dr. Mahitosh Banerjee, Mr. Udit Prasad, Mr. Alok Kumar, Mrs. Babita Faujdar, Mr. Ankit Mishra, Mr. Ritwik Tripathi and Mr. Kunal Singh, for the thought-provoking discussions, support, cooperation and sincere help in many ways.

Finally, I am eternally grateful to my entire family for their faith, patience, encouragement, blessings, and love. I thank my father, Mr. Ganesh Choudhary; my mother, Mrs. Nisha Devi; my brother, Mr. Rahul Kumar; my sister-in-law, Mrs. Tunni Kumari; my sister, Mrs. Priyanka Choudhary; my brother-in-law, Mr. Satyendra Singh; and my niece, Ms. Priushu, for motivating, believing in, and strengthening me to reach new heights. A special thanks to my special family for always being there for me through all the ups and downs.

Date: 6.1.2025

Place: Varanasi

Rohit Kumar

(Rohit Kumar)

Contents

Certificate	i
Declaration by the Candidate	iii
Copyright Transfer Certificate	v
Acknowledgment	viii
List of Tables	xvii
List of Figures	xxi
Nomenclature	xxix
List of Symbols	xxxiii
Preface	xli
1 Introduction	1
1.1 Background overview	1
1.2 Literature Survey	4
1.2.1 Effects of low-frequency oscillations on power system performance	5
1.2.2 Influence of renewable energy sources on power system LFO damping	5
1.2.3 Effect of energy storage systems on LFO damping in power systems	7
1.2.4 Effect of IBR controlled through VSG technique on power system LFO damping	8
1.2.5 Wide-area damping controller for power system	10
1.3 Research Gap and Motivation	12

1.4	Research Objectives	13
1.5	Organisation of the Thesis	14
2	Design and Optimal Location of Power System Stabilizer in the Multi-Machine Power Network	17
2.1	Introduction	17
2.2	Power System Modelling	18
2.2.1	Synchronous generator	18
2.2.2	PSS model	18
2.3	Linearized Model for the Entire System	19
2.4	Classical Damping Torque Analysis Method	20
2.5	PSS Design Based on the CDTA Method	23
2.6	WADC Design Framework	24
2.6.1	Model reduction	25
2.6.2	Feedback signal selection	25
2.6.3	Design of wide-area damping controller	26
2.7	Flowchart of the Proposed Method	26
2.8	Case Study	28
2.8.1	IEEE 9-bus three machine power systems	29
2.8.1.1	Modal analysis	29
2.8.1.2	Mode shape and participation factor	29
2.8.1.3	Selection of the PSS installing locations	30
2.8.1.4	WADC framework for study case-1	33
2.8.1.5	Real-time simulation results	36
2.8.2	IEEE 14-bus five machine power systems	37
2.8.2.1	Modal analysis	38
2.8.2.2	Mode shape and participation factor	38
2.8.2.3	Selection of the PSS installing locations	39
2.8.2.4	WADC framework for study case-2	41
2.9	Summary	44
3	Robust Damping Control for Integrated Wind Turbine Power Networks During Low Inertia Condition	47

3.1	Introduction	47
3.2	Modeling of Power System	48
3.2.1	Modeling of DFIG-based wind turbine system	48
3.2.1.1	Model of drive-train	48
3.2.1.2	Induction generator model	49
3.2.1.3	WTS converter primary controller	49
3.2.2	Power system small signal analysis	51
3.2.2.1	Time delay in feedback signal	52
3.2.2.2	Feedback loop selection	52
3.2.3	The dynamic impacts of WTS integration on system LFO modes .	53
3.3	Design of Dual-Channel WADC for WTS	55
3.3.1	Double-channel control structure and synthesis of H_∞ controller .	55
3.3.2	Procedure to design proposed WADC	56
3.4	Validation on New England Ten-Machine System	57
3.4.1	Description of study system and eigenvalue analysis	57
3.4.2	WTS integration scenario	58
3.4.3	The dynamic impact of control mode in the inter-area mode under the change in system inertia condition	62
3.4.4	Designing WADC for WTS	63
3.4.4.1	Design of double-channel H_∞ WADC	65
3.4.5	Efficacy assessment of the proposed WADC	66
3.5	Real-Time Dynamic Simulation Validations	68
3.5.1	Contingency 1 (C1)	70
3.5.2	Contingency 2 (C2)	74
3.6	Summary	76

**4 Enhancing Damping of Low-Frequency Oscillations in Power Networks
through Energy Storage System-Based Controller 77**

4.1	Introduction	77
4.2	Power system modelling	78
4.2.1	Battery energy storage system model	78
4.2.1.1	Battery pack model	78

4.2.1.2	DC-to-DC bidirectional converter model	79
4.2.1.3	Voltage source converter model	80
4.2.1.4	Control approach for grid-integrated BESS	80
4.2.2	Small-signal analysis	81
4.2.2.1	Time delay in feedback signals	81
4.3	Approach for Choosing the Location, Control Loop, and Feedback Signal for BESS	82
4.3.1	Residue index	82
4.3.2	BESS selection approach	83
4.4	Design of WADC Using Fixed Structure Control Scheme	84
4.4.1	Framework of fixed structure control scheme	84
4.4.2	Fixed-structure H_∞ controller synthesis	85
4.4.3	Procedure to design fixed-structure WADC	86
4.4.4	Flowchart of the proposed scheme	87
4.5	Validation on Modified New England Ten-Machine Benchmark System	87
4.5.1	Study system description and small signal analysis	87
4.5.2	Frequency response of study system	90
4.5.3	Choice of BESS installation position, feedback signal, and damping control loop	91
4.5.4	Design of BESS-based WADC	93
4.5.4.1	Design of fixed-structure H_∞ scheme based WADC for BESS	94
4.5.4.2	Performance evaluation of WADC	95
4.6	Validation of Dynamic Simulation on the Real-Time Digital Simulator	97
4.6.1	Scenario 1 (S1)	98
4.6.2	Scenario 2 (S2)	101
4.6.3	Scenario 3 (S3)	101
4.6.4	Scenario 4 (S4)	104
4.6.5	Effect of nonlinearity on proposed WADC for BESS	106
4.7	Summary	108

5	A Robust Damping Control for Battery Energy Storage Integrated Power Systems to Mitigate Inter-Area Oscillations	109
5.1	Introduction	109
5.2	Power System Modeling	110
5.2.1	Modeling of battery energy storage system	110
5.2.1.1	Battery model	110
5.2.1.2	Modeling of VSC	111
5.2.1.3	Primary control strategy for the BESS	112
5.2.2	Power system model with time delay	112
5.2.2.1	Feedback loop selection for the damping controller	112
5.3	WADC Design Formulation: H_∞ Mixed Sensitivity Control Method .	113
5.3.1	WADC design procedure for BESS	118
5.4	Verification of the WADC Performance on the Modified New England Ten-Machine System	119
5.4.1	Description of the study power system	119
5.4.2	Modal analysis	119
5.4.3	Eigenvalue of study system under different operating conditions using Monte Carlo simulation	122
5.4.4	Location of PSS in inter-area modes	127
5.4.5	Impact of BESS on power system inter-area modes	128
5.4.5.1	BESS control mode dynamic interaction	128
5.4.5.2	Identification of sensitive BESS control parameters on inter-area modes	129
5.4.6	Design of WADC for BESS	130
5.4.6.1	Control loop selection for the WADC	130
5.4.6.2	Design of H_∞ mixed sensitivity scheme-based WADC . . .	131
5.4.7	Performance verification of H_∞ mixed sensitivity scheme based WADC	132
5.4.8	Eigenvalue analysis of the H_∞ mixed sensitivity scheme based WADC under various contingencies	134
5.5	Validation on Real-Time Digital Simulator	136
5.5.1	Disturbance 1 (DS1)	137
5.5.2	Disturbance 2 (DS2)	138

5.5.3	Disturbance 3 (DS3)	139
5.5.4	Control efficacy verification with the integration of renewable source	140
5.5.5	Performance of WADC under variable communication time delay	142
5.6	Summary	145

6 Robust Damping Control Scheme for VSG-Enabled Inverter-Based Resources at Low Inertia Bus in Power Networks to Mitigate Low-Frequency Oscillations **147**

6.1	Introduction	147
6.2	System Modelling	148
6.2.1	VSG topology and principle	148
6.2.2	Inner loop control design of VSG	150
6.2.2.1	Modelling of virtual winding	150
6.2.2.2	Modelling of voltage control loop	151
6.2.2.3	Current limiting control	152
6.2.2.4	Modelling of current control loop	152
6.2.3	Power system model	153
6.3	Damping Analysis of the System with IBRs Controlled via the VSG Technique	153
6.3.1	Study system description	153
6.3.2	Impact on system damping performance for IBRs controlled through VSG technique and grid-following technique	154
6.3.2.1	Damping performance of study system without IBR	155
6.3.2.2	Appropriate location of IBR in the power network	155
6.3.2.3	Damping performance of study system with IBRs	156
6.4	Impact of dynamic interaction between IBRs and power networks on system LFO modes	158
6.4.1	Interaction between active power loop of IBRs and power network	158
6.4.1.1	Interaction between reactive power loop of IBRs and power network	160
6.4.2	Contribution of IBRs state variables in system LFO modes	161

6.5	Supplementary Damping Control Scheme for IBRs	162
6.5.1	Designing a multi-stage mixed H_2/H_∞ scheme-based decentralized damping controller for IBRs	162
6.5.2	Design of supplementary damping control scheme for IBRs	165
6.5.2.1	Multi-stage mixed H_2/H_∞ scheme-based damping con- troller designed for IBRs	165
6.5.2.2	Design of PSS for reactive control loop of IBR	166
6.6	SDC Performance Validation and Dynamic Simulation Analysis	167
6.6.1	Robustness validation of proposed SDC for IBRs	167
6.6.2	Dynamic simulation analysis on RTDS	168
6.6.2.1	Dynamic simulation case-1	168
6.6.2.2	Dynamic simulation case-2	170
6.6.2.3	Dynamic simulation case-3	171
6.6.2.4	Dynamic simulation case-4	172
6.7	Summary	173
7	Conclusions and Future Scope	175
7.1	Summary of important findings	176
7.2	Future scope	177
	References	179
	Appendix-A	191
	Appendix-B	193
	Appendix-C	195
	List of Publications	

List of Tables

2.1	Oscillation modes and damping ratios of study case-1	30
2.2	Sensitivity and damping torque index of study case-1	31
2.3	Eigenvalues of study case-1	33
2.4	Oscillation modes and damping ratios of study case-2	39
2.5	Sensitivity and damping torque index of study case-2	39
2.6	Eigenvalues of study case-2	41
3.1	Eigenvalues and Damping ratio of the study system under CS1 and CS2 .	59
3.2	Damping performance of the inter-area modes under scenario S1 operation of WTS	60
3.3	Damping performance of the inter-area modes under scenario S2 operation of WTS	60
3.4	Damping performance of the inter-area modes under scenario S3 operation of WTS	61
3.5	Damping performance of proposed WADC for system inter-area modes with integration of WTS in Case CS3	67
3.6	Damping performance of proposed WADC for system inter-area modes with integration of WTS in Case CS4	68
3.7	Damping performance of proposed WADC for system inter-area modes with integration of WTS in Case CS5	69
4.1	Power system operating conditions	89
4.2	Damping ratio of the study system in the base case and case1 for different operating conditions	90
4.3	Candidate group of study system	92

4.4	Eigenvalue of system inter-area oscillation modes with WADCs in the candidate group ρ_4 of BESS	96
4.5	Eigenvalue of system inter-area oscillation modes with WADCs in the candidate group ρ_9 of BESS	97
5.1	Operating conditions for the New England ten-machine benchmark system	120
5.2	Eigenvalue of the study system operating under multiple conditions in CS1	121
5.3	Eigenvalue of the study system under multiple operating conditions in CS1 and CS2	121
5.4	Analysis of load variation and damping performance of study system under operating condition OC1	122
5.5	Analysis of load variation and damping performance of study system under operating condition OC2	126
5.6	Analysis of load variation and damping performance of study system under operating condition OC3	126
5.7	Damping performance of the study system with WADCs for inter-area modes in CS2	134
5.8	Damping performance of the study system under different communication delays	135
5.9	Damping performance of the study system under different contingencies . .	136
6.1	Study system LFO modes without IBR	155
6.2	Study system LFO modes with IBRs controlled via $P - Q$ control technique	156
6.3	Study system LFO modes with IBRs controlled via VSG technique	157
6.4	Study system operating uncertainty	167
6.5	Damping performance study system with proposed SDC for IBRs under different operating conditions	168
A.1	Generator data (100 MVA Base)	192
A.2	Generator exciter data	192
A.3	Transformer data	192
A.4	Transmission line data	192
B.1	Generator data (100 MVA Base)	193
B.2	Generator exciter data	194

B.3	Transformer data	194
B.4	Transmission line data	194
C.1	Generator data (1000 MVA Base)	196
C.2	Generator exciter data	196
C.3	Transformer data	196
C.4	Transmission line data	197

List of Figures

2.1	Structure of the PSS.	18
2.2	Block layout of PSS-enabled linearized power systems.	20
2.3	The critical oscillation mode of interest impressed by PSS.	22
2.4	PSS design scheme based on DTI.	23
2.5	Structure of WADC.	24
2.6	Flowchart of the proposed method.	26
2.7	Single line layout of IEEE 9-bus power system with optimal location of PSS and WADC.	29
2.8	Critical LFO mode M2. (a) SG rotor speed-related mode shapes and (b) Participation factor plot	30
2.9	The PSS is to be inaugurated on G2 to affect the critical LFO mode M2.	32
2.10	Hankel singular values corresponding to state linearized model of the IEEE 9-bus system.	34
2.11	Frequency response of reduced-order and full-order models of the IEEE 9-bus system.	34
2.12	Geometric measurement of observability of IEEE 9-bus system.	35
2.13	Parameter of WADC in IEEE 9-bus system.	35
2.14	Real-time simulation framework.	36
2.15	Real-time digital simulation results of IEEE 9-bus system; (a) comparative rotor speed of G2 with different location of PSS, (b) rotor speed of G2, (c) comparison of line active power of line (5-7), (d) active power of line (5-7), and (e) active power of line (3-9).	37
2.16	Single line layout of IEEE 14-bus power system with optimal location of PSS and WADC.	38

2.17	Critical LFO mode M1; (a) SG rotor speed-related mode shapes and (b) participation factor plot.	39
2.18	Hankel singular values corresponding to IEEE 14-bus system state linearized model.	41
2.19	Frequency response of reduced-order and full-order models of the IEEE 14-bus system.	42
2.20	Geometric measurement of observability of IEEE 14-bus system.	43
2.21	Parameter of WADC in IEEE 14-bus system.	43
2.22	Real-time digital simulation results of IEEE 14-bus system; (a) comparative rotor speed of G2 with different locations of PSS, (b) rotor speed of G2, (c) active power of line (5-2), and (d) active power of line (5-4).	44
3.1	DFIG-based WTS configuration and associated control system.	48
3.2	The design scheme for double-channel H_∞ controller.	56
3.3	A modified New England ten-machine system for case CS4 with WTS replacing SG4.	58
3.4	SG participation in the inter-area mode M4 with the integration of WTS operating under scenario S1.	62
3.5	Participation factors of the modified New England ten-machine system in critical inter-area mode. (a) Integration of WTS in CS4 under scenario S1 (b) Integration of WTS in CS5 under scenario S1.	63
3.6	Geometric observability measure for line active power.	64
3.7	Frequency responses of full-order and reduced-order models of the modified New England ten-machine system.	64
3.8	Dynamic response of the system with WTS integration in CS4 operating under scenario S1 for contingency C1. (a) Active power of line 1-39, (b) Rotor speed deviation between SG2 and SG10, (c) DFIG rotor speed, (d) DC-link voltage, (e) d -axis grid side converter reference current, and (f) WTS active power.	71

3.9	Dynamic response of the system with WTS integration in CS4 operating under scenario S2 for contingency C1. (a) Active power of line 1-39, (b) Rotor speed deviation between SG2 and SG10, (c) DFIG rotor speed, (d) DC-link voltage, (e) d -axis grid side converter reference current, and (f) WTS active power.	72
3.10	Dynamic response of the system with WTS integration in CS4 operating under scenario S3 for contingency C1. (a) Active power of line 1-39, (b) Rotor speed deviation between SG2 and SG10, (c) DFIG rotor speed, (d) DC-link voltage, (e) d -axis grid side converter reference current, and (f) WTS active power.	73
3.11	Dynamic response of the system with WTS integration in CS4 operating under scenario S2 for contingency C2. (a) Active power of line 1-39, (b) Rotor speed deviation between SG2 and SG10, (c) DFIG rotor speed, (d) DC-link voltage, (e) d -axis grid side converter reference current, and (f) WTS active power.	75
4.1	A Grid-Connected Battery Energy Storage System with Integrated Control.	79
4.2	Control strategy for Battery Energy Storage System.	80
4.3	Fixed-structure controller standard form model.	84
4.4	Fixed-structure H_∞ control scheme for BESS.	85
4.5	Flowchart of the proposed scheme.	87
4.6	Single-line diagram of the New England 39-bus system integrated with BESS.	88
4.7	Participation factor of synchronous generators in the dominant oscillation mode in the base case under various operating conditions.	89
4.8	Bode plot of the study system: (a) Without BESS, (b) With BESS.	91
4.9	Residue index of study system under operating condition γ_{p4} . (a) BESS installed on Bus-4, (b) BESS installed on Bus-22, and (c) BESS installed on Bus-27.	92
4.10	Frequency responses of the modified New England 39-bus system of full-order and reduced-order system under operating condition γ_{p4}	94

4.11	Dynamic response of the study system with a WADC for BESS in candidate group ρ_4 under various operating conditions: (a) $\Delta\omega_{4-2}$ under γ_{p1} , (b) V_{dc} under γ_{p1} , (c) $\Delta\omega_{4-2}$ under γ_{p2} , (d) V_{dc} under γ_{p2} , (e) $\Delta\omega_{4-2}$ under γ_{p3} , (f) V_{dc} under γ_{p3} , (g) $\Delta\omega_{4-2}$ under γ_{p4} , and (h) V_{dc} under γ_{p4}	99
4.12	Dynamic response of the study system with a WADC for BESS in candidate group ρ_9 under various operating conditions: (a) $\Delta\omega_{4-2}$ under γ_{p1} , (b) V_{dc} under γ_{p1} , (c) $\Delta\omega_{4-2}$ under γ_{p2} , (d) V_{dc} under γ_{p2} , (e) $\Delta\omega_{4-2}$ under γ_{p3} , (f) V_{dc} under γ_{p3} , (g) $\Delta\omega_{4-2}$ under γ_{p4} , and (h) V_{dc} under γ_{p4}	100
4.13	Dynamic response of the study system with a WADC for BESS in candidate groups ρ_4 and ρ_9 under operating condition γ_{p1} : (a) $\Delta\omega_{4-2}$ under ρ_4 , (b) $\Delta\omega_{4-2}$ under ρ_9 , (c) P_{4-14} under ρ_4 , (d) P_{4-14} under ρ_9 (e) P_s under ρ_4 , and (f) P_s under ρ_9	102
4.14	Variable communication time delays.	103
4.15	Dynamic response of the study system with a WADC for BESS in candidate groups ρ_4 and ρ_9 under operating condition γ_{p1} : (a) $\Delta\omega_{4-2}$ under ρ_4 , (b) $\Delta\omega_{4-2}$ under ρ_9 , (c) P_{1-39} under ρ_4 , (d) P_{1-39} under ρ_9 (e) P_s under ρ_4 , and (f) P_s under ρ_9	103
4.16	Modified New England 39-bus system with WADC for BESS and integrated solar PV system on bus-20.	104
4.17	Dynamic response of the studied system integrating BESS and a PV system under operating condition γ_{p1} with WADC for BESS in candidate group ρ_4 : (a) $\Delta\omega_{4-2}$, (b) P_{1-39} , (c) $I_{dref-PV}$ of GSC in PV system, and (d) V_{dc-PV} of PV system.	105
4.18	WADC with nonlinearity for BESS.	106
4.19	Dynamic response of the study system with a WADC linked with nonlinearity for BESS in candidate ρ_4 under operating condition γ_{p1} : (a) P_{1-39} (b) P_s , (c) V_{dc} , and (d) I_{dref}	107
4.20	Dynamic response of the study system with a WADC linked without and with nonlinearity for BESS in candidate ρ_4 under operating condition γ_{p1} : (a) P_{1-39} (b) P_s , (c) V_{dc} , and (d) I_{dref}	107
5.1	Schematic of the BESS integrated power system and associated controls.	111
5.2	Schematic of electrical equivalent battery cell model.	111

5.3	Block diagram for mixed sensitivities control with disturbance signal model.	113
5.4	BESS damping control design strategy.	115
5.5	Flowchart to design WADC for BESS.	118
5.6	A modified New England ten-machine system.	120
5.7	Histogram plot of load variation of study system under operating condition OC1. (a) Bus-3 active power, (b) Bus-3 reactive power, (c) Bus-4 active power, (d) Bus-4 reactive power,(e) Bus-8 active power, (f) Bus-8 reactive power,(g) Bus-12 active power, and (h) Bus-12 reactive power.	123
5.8	Histogram plot of load variation of study system under operating condition OC2. (a) Bus-16 active power, (b) Bus-16 reactive power, (c) Bus-18 active power, (d) Bus-18 reactive power,(e) Bus-21 active power, (f) Bus-21 reactive power,(g) Bus-24 active power, and (h) Bus-24 reactive power. . .	124
5.9	Histogram plot of load variation of study system under operating condition OC3. (a) Bus-25 active power, (b) Bus-25 reactive power, (c) Bus-26 active power, (d) Bus-26 reactive power,(e) Bus-27 active power, (f) Bus-27 reactive power,(g) Bus-29 active power, and (h) Bus-29 reactive power. . .	125
5.10	Participation factor plot of the study system in prominent inter-area oscillation modes.	127
5.11	Contribution of BESS control mode in prominent inter-area modes M2 and M4.(a) System operating on OC1 and (b) System operating on OC2. . . .	128
5.12	BESS control parameters sensitivity to prominent inter-area modes.	129
5.13	GMO of line active power.	130
5.14	Frequency response plot. (a) The modified New England ten-machine system with BESS, (b) Designed WADC for BS1.	132
5.15	Dynamic simulation response of study test system with fixed communication delay of 200 ms under operating condition OC1. (a) Active power on line 1-39, (b) Active power on line 3-18, (c) BS1 converter DC-link voltage, and (d) Rotor speed deviation between SG4 and SG8.	137
5.16	Dynamic simulation response of study test system with fixed communication delay of 200 ms under operating condition OC2. (a) Active power on line 1-39, (b) Active power on line 3-18, (c) BS1 converter DC-link voltage, and (d) Rotor speed deviation between SG4 and SG8.	138

5.17	Dynamic simulation response of study test system with fixed communication delay of 200 ms under operating condition OC3. (a) Active power on line 1-39, (b) Active power on line 3-18, (c) BS1 converter DC-link voltage, and (d) Rotor speed deviation between SG4 and SG8.	139
5.18	The 150 MW wind turbine system and a 150 MW additional load are added to the New England ten-machine system at bus 22.	140
5.19	Dynamic simulation response of study test system with fixed communication delay of 200 ms as well as integration of WTS under operating condition OC1. (a) Rotor speed deviation between SG2 and SG5, (b) Rotor speed deviation between SG5 and SG9, (c) Active power on line 1-39, and (d) DC-link voltage between the grid and the rotor side converter.	141
5.20	WADC for BESS with variable communication time delay.	142
5.21	Variable communication time delay modelled using (5.15).	143
5.22	Dynamic simulation response of study test system with variable communication delay under operating condition OC2. (a) Rotor speed deviation between SG4 and SG8, and (b) Rotor speed deviation between SG2 and SG5.	143
5.23	Dynamic simulation response of study test system with variable communication delay under operating condition OC3. (a) Rotor speed deviation between SG4 and SG8, and (b) Rotor speed deviation between SG2 and SG5.	144
5.24	Dynamic simulation response of the study test system with a proposed WADC, incorporating fixed and variable time delay, under operating condition OC2. (a) Rotor speed deviation between SG4 and SG8, and (b) Rotor speed deviation between SG2 and SG5.	144
6.1	VSG topology and associated supplementary control scheme.	149
6.2	Inner control loop of IBR control via VSG technique.	150
6.3	A New England 39-bus system with IBRs controlled via VSG technique.	154
6.4	Geometric observability measure of the load buses of study system in prominent LFO modes.	156

6.5	Rotor speed mode shape for new LFO mode introduced by IBRs control via VSG technique in New England 39-bus system. (a) Mode $\lambda_{9,10}$, and (b) Mode $\lambda_{11,12}$	158
6.6	Study system with the change of the H of IBRs associated with the VSG technique. (a) Eigenvalue plot, and (b) Damping ratio plot.	159
6.7	Study system with the change of the D_p of IBRs associated with the VSG technique. (a) Eigenvalue plot, and (b) Damping ratio plot.	160
6.8	Study system with the change in k_q of IBRs controlled through the VSG technique. (a) Eigenvalue plot, and (b) Damping ratio plot.	160
6.9	Participation of IBR state variables with virtual inertia constants of 42s and 50s in system LFO modes: (a) IBR 1, and (b) IBR 2.	161
6.10	Damping controller structure: (a) Configuration of mixed H_2/H_∞ scheme, and (b) Multi-stage pole placement region.	163
6.11	The dynamic response of New England 39-bus system with IBR operating under operating condition-1. (a) P_{1-39} , (b) $\omega_5 - \omega_9$, (c) P_{p1} , and (d) V_{cd1}	169
6.12	The dynamic response of New England 39-bus system with IBR operating under operating condition-2. (a) P_{1-39} , (b) $\omega_2 - \omega_{10}$, (c) P_{p1} , and (d) ω_r	170
6.13	The dynamic response of New England 39-bus system with IBR operating under operating condition-3. (a) P_{3-18} , (b) P_{p1} , (c) $\omega_5 - \omega_9$, and (d) f_{G2}	171
6.14	The dynamic response of New England 39-bus system with IBR operating under operating condition-4. (a) P_{5-12} , (b) P_{p1} , (c) $\omega_5 - \omega_9$, and (d) $\omega_6 - \omega_3$	172
A.1	Single line diagram of IEEE 9-bus power system.	191
B.1	Single line diagram of IEEE 14-bus power system.	193
C.1	Single line diagram of New England 39-bus system.	195

Nomenclature

List of Abbreviations

IBRs	Inverter-Based Resources
RESs	Renewable Energy Sources
WTS	Wind Turbine System
PV	Photovoltaic
ESS	Energy Storage System
BESS	Battery Energy Storage System
SOC	State of Charge
SMES	Superconducting Magnetic Energy Storage System
VSG	Virtual Synchronous Generator
LFOs	Low-Frequency Oscillations
SGs	Synchronous Generators
PSS	Power System Stabilizer
WAPSS	Wide-Area Power System Stabilizer
WADC	Wide-Area Damping Controller
PMUs	Phasor Measurement Units
SDC	Supplementary Damping Controller

FACTS	Flexible AC Transmission Systems
POD	Power Oscillation Damping controller
STATCOM	Static Synchronous Compensator
GFC	Grid Forming Control
PSO	Particle Swarm Optimization
ATDC	Adaptive Time-Delay Compensator
MMPN	Multi-Machine Power Network
CDTA	Classical Damping Torque Analysis
DTI	Damping Torque Index
GMO	Geometric measurement of Observability
PF	Participation Factor
SI	Sensitivity Index
BT	Balanced Truncation
RTDS	Real Time Digital Simulator
GTSYNC	Giga-Transceiver Synchronization Card
RPS	Rest Part of Power System
VSC	Voltage Source Converter
RSC	Rotor Side Converter
GSC	Grid Side Converter
PCC	Point of Common Connection
APC	Active Power Controller
RPC	Reactive Power Controller

BC	Base case
CS1	Case-1
CS2	Case-2
CS3	Case-3
C1	Contingency-1
C2	Contingency-2
S1	Scenario-1
S2	Scenario-2
S3	Scenario-3
S4	Scenario-4
OC1	Operating Condition-1
OC2	Operating Condition-2
OC3	Operating Condition-3
DS1	Disturbance-1
DS2	Disturbance-2
DS3	Disturbance-3

List of Symbols

δ	Rotor angle
ω_s	Synchronous speed
E'_q	q -axis transient internal voltage
E_{fd}	Field voltage
D	Damping coefficient
T_M	Mechanical input torque
H	Machine inertia constant
I_d, I_q	d -axis and q -axis stator current
X_d, X'_d	d -axis reactance and q -axis transient reactance
T'_{do}, T'_{qo}	d -axis and q -axis transient flux decay constant
V_t	Terminal voltage
V_{ref}	Reference voltage
K_A, T_A	Gain and time constant of the exciter
m	Number of SG
B_L	Transfer function matrix from Δu_s to state variables
Δu_s	Output signal of the stabilizer
Δy_s	Stabilizer feedback signal

F_{PSS}	Forward path from the PSS controlling signal to the electro-mechanical oscillation loop of the SG
T_{PSS}	Transfer function of the PSS
D_{PSSKL}	Damping coefficient in the electromechanical oscillation loop of SG
T_{PSSKL}	Electric torque contribution from the PSS to the electro-mechanical oscillation loop of all SG
γ_L	Reconstructed function
$\angle\varphi_L$	SG critical LFO loop angle
$\angle\phi$	Compensation angle
λ_K	Critical LFO mode
p	Differential operator
ω_t	Speeds of the wind turbine
ω_r	Speeds of the Induction generator
ω_e	Speeds of the synchronous reference frame
H_t	Inertia constant of wind turbine
D_{tg}	Damping coefficients between the generator and wind turbine
D_t	Wind turbine damping coefficient
K_{tg}	Drive train shaft stiffness coefficient
D_g	Damping coefficient of the induction generator
T_g	Electromagnetic torque of the induction generator
T_m	Wind turbine mechanical torque
β	Wind turbine pitch angle
λ	Wind turbine tip speed ratio
C_p	Power coefficient of the wind turbine blade

R	Wind turbine rotor radius
ρ	Air density
V_w	Wind speed
P_m	Wind turbine mechanical power
ω_b	Base angular velocity
ω	Rotational speed of the arbitrary reference frame
x_m	Magnetizing reactance of the induction generator
x'_{rr}	Rotor reactance of the induction generator
r'_r	Rotor resistance of the induction generator
r_s	Stator resistance of the induction generator
$\psi_s, \& \psi'_r$	Stator and rotor fluxes of the induction generator
$V_s, \& V'_r$	Stator, and rotor voltages of the induction generator
$P_{sref}, \& Q_{sref}$	Active and reactive power reference of RSC in WTS
$P_s, \& Q_s$	Active and reactive power of WTS
$u_p, \& u_q$	Damping control signal of the WADC
$K_{pr1}, \& K_{ir1}$	Proportional and integral gain coefficients of the PI controller of the RSC outer control loop for active power control loop
$K_{pr3}, \& K_{ir3}$	Proportional and integral gain coefficients of the PI controller of the RSC outer control loop for reactive power control loop
$I_{drref}, \& I_{qrref}$	dq -axis reference current generation for RSC
$I_{dr}, \& I_{qr}$	dq -axis rotor current of RSC
$K_{pr2}, \& K_{ir2}$	Proportional and integral gain coefficients of the PI controller of the RSC inner control loop for active current control loop
$K_{pr4}, \& K_{ir4}$	Proportional and integral gain coefficients of the PI controller of the RSC inner control loop for reactive current control loop

$V_{dr}, \& V_{qr}$	dq -axis RSC voltages
V_{dc}	DC-link voltage
V_{dcref}	Reference voltage of voltage control loop of GSC
$Q_{gref} \& Q_g$	Reactive power reference and reactive power of GSC in WTS
$K_{pg1}, \& K_{ig1}$	Proportional and integral gain coefficients of the PI controller of the GSC outer control loop for voltage control loop
$K_{pg3}, \& K_{ig3}$	Proportional and integral gain coefficients of the PI controller of the GSC outer control loop for reactive power control loop
$I_{dgref}, \& I_{qgref}$	dq -axis reference current generation for GSC
$I_{dg}, \& I_{qg}$	dq -axis current of GSC
$K_{pg2}, \& K_{ig2}$	Proportional and integral gain coefficients of the PI controller of the GSC inner control loop for voltage current control loop
$K_{pg4}, \& K_{ig4}$	Proportional and integral gain coefficients of the PI controller of the GSC inner control loop for reactive current control loop
Δ	Small deviation
$x, u \& y$	Power system state, input, and output vectors
$A, B, C, \& D$	Power system system, input, output, and feed-forward matrices
$m, n, \& o$	Power system state, input, and output variables
T_d	Delay time
λ_i	LFO mode
$gm_{oj}(i)$	GMO of i^{th} oscillation mode
φ_i	Right eigenvector of i^{th} oscillation mode
$\ \ , \& $	Euclidean norm and modulus
P_L	Real power flow through transmission line
w	External input

K	Transfer function of the controller
T	Transfer function for generalized plant
z	Regulated variables
v	Measure output
M_{zw}	Closed-loop transfer function from w to z
V_1	Battery pack terminal voltage
I_L	Inductor current
I_{dc}	DC-link current
V_b	Battery cell voltage
R_b	Battery internal resistance
α_1	Bidirectional converter duty cycle
$C_1, C_2, \& L$	Converter capacitance and inductance
$V_{sd}, \& V_{sq}$	dq - axis grid voltage or PCC voltage of VSC
$V_{cd}, \& V_{cq}$	dq - reference frame voltages of VSC
$m_d, \& m_q$	Modulation index of VSC in dq reference frame
$V_s, V_c, \& I_c$	Grid voltage, VSC voltage, and VSC current
$L_V, \& R_V$	Aggregated inductance and resistance of the VSC, transformer, and filter
C_V	Filter capacitance
$V_{cd}, \& V_{cq}$	Pulse width modulation control signal for VSC
$I_{cd}, \& I_{cq}$	dq - axis current of VSC
$I_{cdref}, \& I_{cqref}$	dq - axis reference current generation for inner current control loop of VSC

$K_{pp}, \& K_{ip}$	Gain coefficients of the PI controller in the outer active control loop of the VSC
$K_{pq}, \& K_{iq}$	Gain coefficients of the PI controller in the outer reactive control loop of the VSC
$K_{picd}, \& K_{iicd}$	Gain coefficients of the PI controller in the inner active current control loop of the VSC
$K_{picq}, \& K_{iicq}$	Gain coefficients of the PI controller in the inner reactive current control loop of the VSC
$G(s)$	Transfer function of system
R_i	Residue index
$N_i^T, \& M_i$	Left and the right eigenvector matrices related to the eigenvalue λ_i
M_p	Consequence of the choice
ρ	Set of each candidate's installation positions, feedback signals, and control loops
γ_0	Steady-state operating condition
γ_p	Operating condition
$\Phi(\gamma)$	Collection of various operating conditions
$V_1, \& V_2$	Voltage drops across $R_1 \parallel C_1$ and $R_2 \parallel C_2$
R_{in}	Charge transfer resistance
V_{oc}	Open circuit voltage
V_b	Terminal voltage of the battery cell
I_b	Battery cell current
$S(s)$	Sensitivity function
$K(s)S(s)$	Complementary sensitivity functions
G_{dp}	Transfer function for the open-loop plant model of the system
$I_{ds}, \& I_{qs}$	Point of coupling current in d - q axis

$x_{pll}, \& \theta_{pll}$	PLL state variables
$x_{p1}, \& x_{q1}$	Power control loop states of VSC
$x_{p2}, \& x_{q2}$	Current control loop states of VSC
d	Disturbance signal
$W_1(s), \& W_2(s)$	Shaping filter (low pass and high pass filter)
$W_{2h}(s)$	Small constant or high pass filter
x_k	Damping controller state vector
$A_k, B_k, C_k, \& D_k$	Damping controller system state, input, output, and feed-forward matrices
r	Reference signal for damping controller
X	Real symmetric matrix
$R_1, S_1, M_1, \& N_1$	Sub-matrices of X
ζ_{min}	Minimal damping ratio
θ	Conic sector angle
θ_r	Reference angle
V^*	Voltage magnitude of virtual AVR for VSG
V_s	Voltage magnitude of PCC
$\omega_{VSG}, \& \omega_o$	VSG angular frequency and grid angular frequency
D_q	Droop coefficient of the Q - V loop
$K_q, \& V^*$	Reactive power adjustment coefficient, and output voltage of the virtual excitation loop
$x_1, \& x_2$	Voltage control loop state variables of IBR
$K_{ivd}, \& K_{ivq}$	Integral gain coefficient of the voltage control loop of VSG control in the dq reference frame

$K_{pvd}, \& K_{pvq}$	Proportional gain coefficient of voltage control loop in the dq reference frame
$x_3, \& x_4$	Current control loop state variables of IBR
$x_{VSG}, \& u_{VSG}$	state vector, and input vector for the state model of IBR controlled through the VSG technique
y_{VSG}	Output vector for the state model of IBR controlled through the VSG technique
$A_{VSG}, \& B_{VSG}$	System and input matrices coefficient of state model of IBR controlled through the VSG technique
$V_{VSG}, \& D_{VSG}$	Output and feed-forward matrices coefficient of state model of IBR controlled through the VSG technique
$P_p(s)$	Power system model that includes the parameters perturbation of the proportional gain coefficient of the voltage control loop of IBRs
$G_p(s)$	Power system model without the IBRs control loop perturbations
$\Delta(s)$	Perturbation block
$Z_2, \& Z_\infty$	Output channel of H_2/H_∞ damping controller
$H_2, \& H_\infty$	$H_2, \& H_\infty$ are performance channel of H_2/H_∞ damping controller
D_r	Pole placement region
$A_\infty, \& A_2$	Weight of the H_∞ and H_2 performance channel
$\ M_{wz_2}(s)\ _2$	H_2 norm
$\ M_{wz_\infty}\ _\infty$	H_∞ norm

Preface

Power system networks are interconnected, nonlinear, and extremely complex systems susceptible to various events that might cause Low-Frequency Oscillations (LFOs), which may affect the system's stability. These LFOs, which occur at a frequency lower than 2 Hz, are frequently caused by events such as line failures, abrupt load changes, and generator output power variations. The LFOs must be damped out as quickly as possible to make the system stable and dependable because they are harmful. Consequently, reducing power oscillations through Power Oscillation Damping (POD) controller and installing Power System Stabilizers (PSSs) on Synchronous Generators (SGs) are two conventional methods for damping LFOs in multi-machine power systems. PSSs are designed to enhance system stability by providing additional damping to generator rotor oscillations through modulation of the excitation system. However, PSSs primarily utilize local signals, which limits their effectiveness in damping inter-area oscillation modes due to a lack of global observability.

To address the limitations of PSSs in damping inter-area oscillations, a robust Wide-Area Damping Controller (WADC) is introduced. WADCs use wide-area measurements, such as Phasor Measurement Unit (PMU) data, to provide a broader view of the system's dynamic behaviour. By using these wide-area signals, WADC can effectively dampen inter-area oscillations, enhancing the overall stability of the interconnected power system. This approach ensures sufficient damping across the network, mitigating the adverse effects of LFOs and maintaining system reliability.

WADC can be designed using robust control strategies, such as H_∞ , mixed sensitivity H_∞ , and H_2/H_∞ control, to effectively handle uncertainties and varying system conditions. These controllers are designed to provide sufficient damping even when system parameters change or when faced with model inaccuracies. Various actuators, including wind energy conversion systems, solar photovoltaic systems, energy storage systems, and

virtual synchronous generators, are utilized in WADC designs to mitigate system inter-area oscillations and enhance the system's dynamic performance. A brief literature survey on low-frequency oscillations under Renewable Energy Sources (RESs) and Inverter Based Resources (IBRs) integration, various control strategies to damp these oscillations, motivation behind work carried out in this thesis based on research gap, and formulated research objectives are presented in first Chapter.

The second Chapter of the thesis presents the Damping Torque Index (DTI) for determining the optimal installation location of PSS in a multi-machine power network. The selection criteria for the PSS location are based on the maximum magnitude of the DTI under normal operating conditions, ensuring that the PSS is placed where it can provide the most effective damping. The parameters of the PSS are adjusted using the phase compensation methodology to optimize its performance. Additionally, a reduced-order model-based WADC is designed and installed at the synchronous generator, where the optimal PSS is located. This approach aims to enhance the damping of LFOs in the system, thereby improving overall system stability and performance.

The increased penetration of RESs into power systems significantly impacts the damping of LFOs. RESs, such as Wind Turbine Systems (WTS), inherently differ from traditional synchronous generators in their contribution to system inertia and damping characteristics. The intermittent and variable nature of RESs often reduces system inertia, which can exacerbate LFOs and pose stability challenges. This decrease in inertia diminishes the natural damping usually provided by synchronous machines, making the power system more susceptible to oscillatory instability.

The third Chapter of the thesis investigates the impact of inter-area oscillation damping in power systems under low system inertia conditions caused by a high penetration of WTS operating in sub-synchronous, normal, and super-synchronous scenarios. This work examines the effects of replacing a synchronous generator with a WTS of the same MVA capacity on system dynamics, mainly focusing on the emergence of new critical modes of inter-area oscillations that can affect system stability. It explores the dynamic interactions between WTS and SGs and their impact on inter-area oscillations. This work proposed a reduced-order model-based double-channel WADC for WTS to address these challenges, utilizing an H_∞ control scheme. This WADC is designed to damp prominent oscillation modes effectively and mitigate the adverse effects of reduced

system inertia. The real-time feasibility of the proposed double-channel H_∞ WADC is validated using the Real-Time Digital Simulator (RTDS) platform.

The application of Energy Storage Systems (ESSs) in power systems is pivotal for enhancing the damping of inter-area oscillations, which is essential for maintaining grid stability amidst the increasing integration of renewable energy sources. ESS provides rapid and precise control over active and reactive power, helping to stabilize grid frequency and dampen oscillations, particularly in regions prone to variability due to renewables. The strategic deployment of ESS in the grid allows operators to quickly mitigate frequency deviations by injecting or absorbing power, thus preserving system inertia and damping characteristics that might be compromised by integrating renewable energy sources.

Furthermore, ESS can operate independently or in conjunction with other stabilization technologies, such as PSS and WADC, to ensure optimal damping without compromising overall grid reliability. In addition to damping oscillations, ESS provides critical ancillary services, including frequency regulation, voltage support, and load balancing, which are essential for maintaining stability in environments with high renewable energy penetration. These capabilities make ESS a crucial component in modern power systems, enhancing flexibility and resilience in managing the dynamic challenges posed by renewable energy integration.

Mitigating inter-area LFOs is crucial for maintaining power system stability. These oscillations are closely tied to power oscillations, and adequate power modulation through the Battery Energy Storage System (BESS) can help preserve stability. The fourth Chapter of this thesis proposes a strategy for selecting the optimal location for BESS placement based on the maximum of all minimal residue indices under varying system loading conditions. This method determines the best location for the BESS, the appropriate feedback signal, and the suitable damping control loop (i.e., active or reactive power control) for implementing a supplementary damping controller. A reduced-order model-based fixed-structure H_∞ scheme-based WADC is proposed to enhance the damping performance for system LFOs. The robust damping performance of the designed controller is validated on the RTDS under different contingencies, including varying system operating scenarios, uncertainties associated with fixed and variable communication delays in the feedback signal, nonlinearities in the damping control loop, and the integration of renewable sources such as solar photovoltaic (PV) systems.

The fifth Chapter of this thesis examines the impact of multiple BESSs on inter-area oscillations in the power system under varying loading conditions to study the impact of dynamic interaction between the BESS control modes and synchronous generators, along with BESS control parameters, on the damping of prominent inter-area oscillations. Further, WADC based on an H_∞ mixed sensitivity scheme is proposed for BESS. This controller, designed using the Linear Matrix Inequality (LMI) framework, aims to mitigate prominent inter-area oscillations. The sensitivity to variations in BESS control parameters is used to determine optimal location for supplementary damping controller. The RTDS platform is used to assess the real-time effectiveness of the proposed WADC, with simulation results demonstrating that the controller significantly reduces several inter-area oscillation modes.

In RES-based generation, IBR is used to supply power to the grid. However, the increasing integration of RES-based generation in modern power systems reduces grid inertia and damping performance because IBR lacks inherent rotating inertia. This issue is especially significant when RES are integrated into the grid through IBR, given their high voltage levels and large power capacities. Conventional grid-following controls for IBR do not provide inertia support, which can lead to stability problems and pronounced oscillations from minor disturbances, potentially compromising frequency stability. The Virtual Synchronous Generator (VSG) control technique addresses this issue by emulating the inertia of synchronous generators, thereby improving grid stability and reducing these challenges.

The sixth Chapter of this thesis presents the impact of IBRs controlled through the VSG technique on power system LFOs. It investigates how dynamic interactions between the power network and the active and reactive power loops of IBRs, with varying parameters such as inertia constant (H), damping coefficient (D_p), and voltage gain coefficient (k_q), influence LFO damping. Further, the Supplementary Damping Controller (SDC) scheme for IBRs is proposed to enhance system LFOs damping and mitigate the power oscillations of IBRs. This SDC comprises a multi-stage mixed H_2/H_∞ decentralized damping controller linked with the IBR's active control loop and the PSS linked with the reactive control loop of the IBR. The robustness of the proposed SDC is validated using RTDS simulations under various operating conditions, including load changes, network topology adjustments, and the integration of renewable sources. The simulation results

demonstrate that the proposed SDC effectively mitigates both system LFOs and power oscillations in IBRs. Finally, the seventh Chapter concludes the thesis by summarizing key findings and suggesting directions for future research.